Interpolation-Based Gray-Level Co-Occurrence Matrix Computation for Texture Directionality Estimation

Marcin Kociolek
Institute of Electronics
Lodz University of Technology
ul. Wolczanska 211/215, 90-924 Lodz, Poland
Email: marcin.kociolek@p.lodz.pl

Peter Bajcsy, Mary Brady and Antonio Cardone
National Institute of Standards and Technology
Software and Systems Division
100 Bureau Drive, 20899 Gaithersburg, MD, USA
Emails: peter.bajcsy@nist.gov,
mary.brady@nist.gov, antonio.cardone@nist.gov

***Abstract*—A novel interpolation-based model for the computation of the Gray Level Co-occurrence Matrix (GLCM) is presented. The model enables GLCM computation for any real-valued angles and offsets, as opposed to the traditional, lattice-based model. A texture directionality estimation algorithm is defined using the GLCM-derived correlation feature. The robustness of the algorithm with respect to image blur and additive Gaussian noise is evaluated. It is concluded that directionality estimation is robust to image blur and low noise levels. For high noise levels, the mean error increases but remains bounded. The performance of the directionality estimation algorithm is illustrated on fluorescence microscopy images of fibroblast cells. The algorithm was implemented in C++ and the source code is available in an openly accessible repository.**

I. Introduction

Gray Level Co-occurrence Matrix (GLCM) computations are frequently used to capture second-order statistics of image textures [1], [2], [3]. GLCMs are calculated over a selected image region by counting the number of co-occurring intensity pairs. Locations of the co-occurring pixels under consideration are defined by fixed angle and offset (distance) values. Given an image, the values of angle and offset are constrained by a lattice consisting of integer row and column locations of image pixels. The lattice constraints introduce uncertainty in the GLCM computation, since only specific angle-offset pairs correspond to the image lattice.

The gap between lattice-constrained and real-valued computations of GLCM motivates our work. A summary of a few software packages with GLCM computation is provided in Table I. They are constrained by the lattice and somehow limited to specific offset values and direction angles, according to the seminal GLCM paper [4]. However, GLCM computations should be applicable for any direction of interest, which motivates the need for any real-valued angle and offset.

From an application perspective, texture directionality estimation techniques are extremely useful in cell biology. For example, the assembly mechanisms of stress fibers in response to mechanical characteristics of the extracellular matrix are related to cardiovascular diseases [10], [11]. However, microscopy images of cells are frequently being obfuscated by cell clutter. In this context, the robustness of directionality estimation with respect to noise and image blur needs to be assessed.

TABLE I
A summary of GLCM angle and offset parameters allowed in various software packages supporting GLCM computations (LC - lattice constrained).

Software	Available angle	Available offsets
QMaZda [5]	0, 45, 90, 135	1,2,3,4,5
MATLAB [6]	0, 45, 90, 135	Any (LC)
ImageJ/FIJI plugin [7]	0, 45, 90, 135	Any (LC)
WIPP [8]	Any (LC)	Any (LC)
Pythonxy/scikit-img [9]	Any (LC)	Any (LC)

The aforementioned motivations and needs can be summarized into two objectives. The first objective is to enable the computation of GLCM derived features over any real-valued angles and offsets that are not constrained to an image lattice. The second objective is to assess the performance of GLCM derived features on texture directionality estimation in terms of robustness to blur and noise.

After a brief overview of related work in Section II the above objectives are addressed by defining an interpolation-based GLCM computation that can operate on any real-valued angle and offset pair (Section III-A), designing a method for estimating texture directionality from GLCM derived features (Section III-B), and evaluating its robustness with respect to image noise and blur on synthetic images (Section IV). The method is compared with the Fiji implementation of a Fourier Transformation (FT)-based directionality estimation technique [12] (Section IV-D), and it is demonstrated on fluorescence microscopy images of fibroblast cells (Section IV-E). Section V discusses this work and suggests future directions.

II. Previous work

Texture directionality estimation has been explored based on Radon [13], Moijete [14], and Fourier transforms [15], or on the auto-covariance function [16]. However, such approaches require a mapping between the visual perception of

directionality and its characteristics in the transformed space. GLCM is more directly linked to human visual perception [17]. Past work on seismic image data [18] and on the characterization of collagen fibers [19] shows that GLCM derived homogeneity and energy features are maximal when computed along the perceived texture directionality. This property of GLCM derived features was also pointed out in [20]. However, GLCM computations are traditionally limited to a small set of direction and offset pairs, since pair values defining the locations of the co-occurring pixels belong to the lattice consisting of integer row and column locations of image pixels.

III. Methods

In this section, we define an interpolation-based GLCM computation. Then, a texture directionality estimation algorithm is designed using the interpolation-based GLCM.

A. Interpolation-based GLCM Computation

The mathematical notations introduced by Haralick[4] are used here. Let us define an image I that is a mapping from a lattice of pixels to integer values of gray level intensities. The mapping assigns a set of quantized (or binned) gray levels $G = \{0, 1, 2, , N_G\}$ to each lattice point defined by $L_Y = \{0, 1, 2, , N_Y\} \times L_X = \{0, 1, 2, , N_X\}$. Thus, an image I is defined as a mapping $I : L_Y \times L_X \rightarrow G$. According to [4], the lattice-based GLCM entry at i-th row and j-th column $C(i, j, d, \alpha)$ is defined for angles $\alpha = 0°, 45°, 90°$ and $135°$ at a distance (i.e., offset) d as follows:

$$\begin{aligned} &C(i,j,d,\alpha) = \\ &= \#\Big\{\big((k,l),(m,n)\big) \in (L_Y \times L_X)\times \\ &\times(L_Y \times L_X)\Big| I(k,l) = i,\ I(m,n) = j, \\ &|k-m| = V1(\alpha),\ |l-n| = V2(\alpha)\Big\} \end{aligned} \tag{1}$$

where the symbol # refers to the number of elements in the set, and the four angles $\alpha = 0°, 45°, 90°$ and $135°$ correspond to the following four combinations of the $V1, V2$ values:

$$\begin{array}{ll} \{V1(0°) = 0; & V2(0°) = d\} \\ \{V1(45°) = d; & V2(45°) = -d\} \\ \{V1(90°) = d; & V2(90°) = 0\} \\ \{V1(135°) = -d; & V2(135°) = -d\} \end{array}$$

applied to the lattice location coordinates k, l, m and n. The GLCM is of size $N_G \times N_G$. The GLCMs in [4] are defined to be symmetric, which implies $C(i, j, d, \alpha) = C(j, i, d, \alpha)$. The quantization (binning) into N_G gray levels is carried out as in Eq. (2).

$$\begin{aligned} G\big(I(i,j)\big) = &\left[\frac{I(i,j) - min_{(k,l)\in I} I(k,l)}{max_{(k,l)\in I} I(k,l) - min_{(k,l)\in I} I(k,l)}\right] \in \\ &\in \{0, 1, \ldots, N_G\} \end{aligned} \tag{2}$$

The operations min and max are performed over the entire image I, and G is the quantized gray level of an intensity $I(i, j)$.

Interpolation-based rather than lattice-based GLCM computations are introduced here. The general element of the interpolation-based GLCM at i-th row and j-th column is defined below for a given interpolation model $Model$, real-valued angle α and offset d.

$$\begin{aligned} &C(i,j,d,\alpha,Model) = \\ &= \#\Big\{\big((k,l),(m = k + d\ cos(\alpha), \\ &n = l + d\ sin(\alpha)\big) \in (L_Y \times L_X)\times \\ &\times(\mathbf{R}_Y \times \mathbf{R}_X)\Big| I(k,l) = i\ \& \\ &\&\ Interpolated\ I(m,n,Model)\Big\} \end{aligned} \tag{3}$$

where the symbol # refers to the number of elements in the set and $InterpolatedI(m, n, Model)$ denotes the interpolated intensity for the real-valued location $(m, n) \in (\mathbf{R}_Y \times \mathbf{R}_X)$. The bilinear interpolation model is used in this work. The main idea behind the interpolation-based GLCM computation is that, by definition, lattice constraints limit the direction/offset pairs that must be considered. In the proposed approach one of the two points needed for GLCM calculation is in the image lattice and the second one is interpolated (Fig. 1).

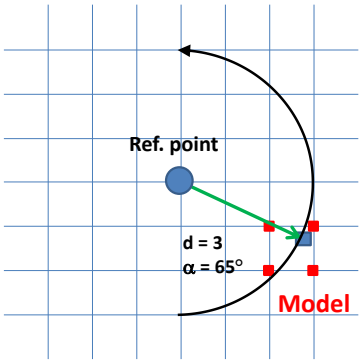

Fig. 1. Instance of interpolation-based GLCM computation. Locations in blue represent a reference point on the lattice and an interpolated point located at distance $d = 3$ and angle $\alpha = 65°$. The intensity value at the latter point is obtained by bilinear interpolation over the 4 closest neighbors (in red)

B. Texture directionality estimation algorithm based on GLCM derived features

Four GLCM features, originally implemented in MatLab software [21], are considered in this paper: homogeneity, contrast, correlation, and energy. Those features are modified below to take into account the interpolation-based GLCM, by simply substituting $C(i, j, d, \alpha)$ with $C(i, j, d, \alpha, model)$.

$$\begin{cases} homogeneity & = \sum_{i,j\in[1,G]} \frac{C(i,j,d,\alpha,model)}{1+|i-j|} \\ contrast & = \sum_{i,j\in[1,G]} |i-j|^2 C(i,j,d,\alpha,model) \\ correlation & = \sum_{i,j\in[1,G]} \frac{(i-\mu_i)(j-\mu_j)C(i,j,d,\alpha,model)}{\sigma_i\sigma_j} \\ energy & = \sum_{i,j\in[1,G]} C(i,j,d,\alpha,model)^2 \end{cases} \tag{4}$$

The characteristics of the GLCM features in Eq. (4) with respect to texture directionality were tested for a set of fixed offset values on synthetic images consisting of bars of various thicknesses and orientations. A total of 1320 tests were performed. GLCM features were generally maximal or

minimal along the bar direction and in overall agreement with the previous studies [18], [19] and [20]. Specifically, correlation was maximal in 99% of the cases, contrast was minimal in 99%, homogeneity was maximal in 95%, and energy was maximal in 68%. According to these results, correlation and contrast seem to be the most reliable features for texture directionality estimation. Correlation is used for the texture directionality estimation algorithm defined in this paper. Fig. 2 shows an instance of the above-mentioned tests, where GLCM features are plotted for 4 offset values and over 181 direction angles $\alpha \in \{0°, 1°, \ldots, 180°\}$. In this case, three GLCM features reach their maximum or minimum value in correspondence of the actual texture directionality, which is $\alpha = 101°$. Only GLCM energy does not follow this behavior.

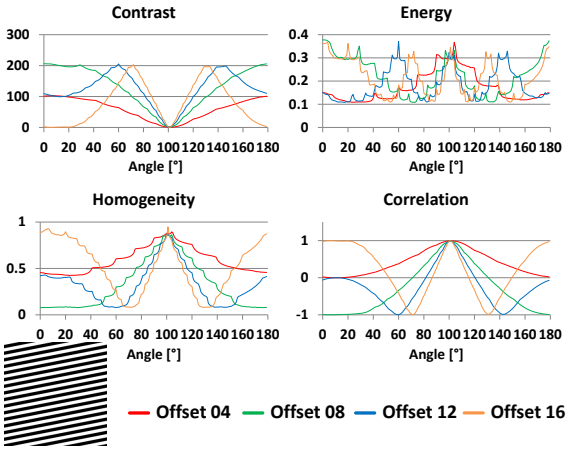

Fig. 2. The four texture features derived from the interpolation-based GLCM are plotted in function of the computation angle, for four offset values. The GLCM is computed on a synthetic texture containing 8-pixel wide bars, 8-pixel spaced, oriented at 101° with respect to the vertical axis (inset).

The algorithm for texture directionality estimation is defined as follows. Observe that there are no restrictions on the size and shape of the processed image region. Let A and D be respectively the set of angles and offsets to use for the interpolation-based GLCM computation. Let $F(\alpha, d, Model)$ be the GLCM correlation feature from Eq. (4), where α and d belong to sets A and D, and $Model$ represents the interpolation model. Then, TEXT_DIR_DETECT algorithm consists of the steps below:

1) For each $d \in D$, compute GLCM based correlation $F(d = const, \alpha)$ over every $\alpha \in A$.
2) Find the angle $\alpha_{max}(d)$ corresponding to the maximum, value of $F(d, \alpha)$ for a given offset d.
3) Find the highest occurrence of angle $\bar{\alpha}$ among the $\alpha_{max}(d)$ for all $d \in D$. The angle $\bar{\alpha}$ represents the detected texture directionality.

The outputs of Step 2 and 3 of the above algorithm can be formally defined as $\alpha_{max}(d) = \arg\max_{\forall \alpha \in A} F(d, \alpha)$ and $\bar{\alpha} = Mo\{\alpha_{max}(d)\}_{d \in D}$ where Mo is the mode of the set in parenthesis for every $d \in D$. Note that if no unique mode is found then texture directionality is not reported which is a valid outcome of the algorithm. The described TEXT_DIR_DETECT algorithm was implemented in C++ using the OpenCV image processing library, and the source code is available in the GitHub repository [22].

IV. Performance Tests and Examples of Applications

A. Definition of synthetic images and procedure for tests

The robustness of our texture directionality estimation algorithm with respect to noise and image blur was evaluated on synthetic texture images with depth of 16 bits per pixel (BPP), with dimension of 512×512 pixels and with known directionality, which were obtained as follows. Initially, evenly spaced vertical bars were built, with thickness and spacing equal to 8, 12 and 16 pixels, with background intensity equal to 16384 (1/4 of the full scale), and with foreground intensity equal to 49151 (3/4 of the full scale). Next, the bars were rotated of angles $0°, 1°, \ldots, 90°$,counterclockwise with respect to the vertical direction. Please observe that, in general, a given rotation involves the interpolation of the foreground intensity values, which leads to multiple grayscale values for the rotated image. This procedure yielded 273 images (91 directions by 3 bar thicknesses). In order to evaluate the robustness of the texture directionality estimation algorithm to noise, the synthetic images were perturbed using the Gaussian PDF noise with zero average and standard deviation $\sigma = \{2000, 4000, \ldots, 20000\}$. On the other hand, in order to evaluate the robustness of the texture directionality estimation algorithm to blur, the synthetic images were perturbed by filtering with square averaging kernels of size $\{3 \times 3, 5 \times 5, \ldots, 21 \times 21\}$ pixels. Instances of the obtained synthetic images are shown in Fig. 3 in pseudo colors, so that the intensity values can be seen more clearly.

Based on the above, a total of 3003 synthetic images was obtained after noise perturbation ($3 barthickness \times 91 directions \times 11 noisestandarddeviationlevels$), and the same number of synthetic images was obtained after blur perturbation ($3 barthickness \times 91 directions \times 11 blurkernelssize$). On each synthetic image 121 circular regions of interest (ROIs) with diameter of 61 pixels, regularly spaced and partially overlapping to fully cover each synthetic image, were used to perform the directionality estimation. Circular ROIs were chosen because they are not expected to bias in any way the directionality detection, unlike square or rectangular ROIs. Ultimately, our tests yield a total of 11011 directionality estimates ($121 ROIs \times 91 directions$) for each bar thickness and perturbation level. Our texture directionality estimation algorithm was applied to the synthetic images described above. The directionality estimation was carried out using 1° sampling and the GLCM was computed using 16 intensity bins. Two metrics to evaluate the algorithm performance were employed: the mean value and the maximum value of the directionality detection error (DDE). The DDE is defined as the absolute value of the difference between the estimated directionality $\bar{\alpha}$ and the known directionality α of a synthetic texture image, as formally shown in Equation (5).

$$DDE = |\bar{\alpha} - \alpha| \tag{5}$$

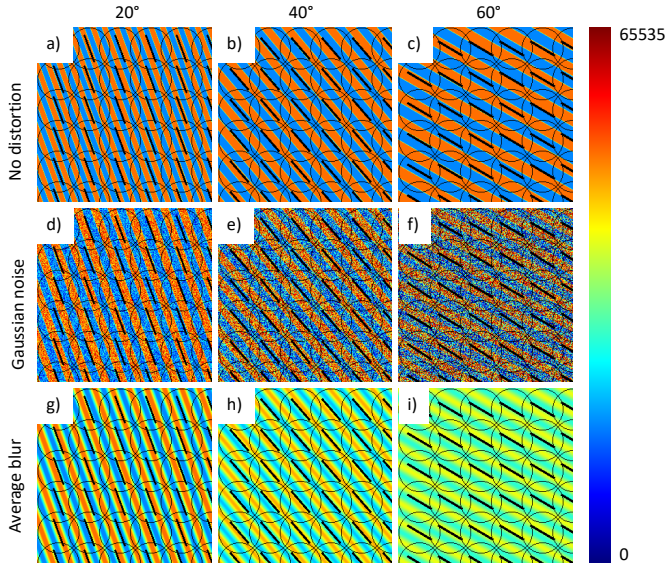

Fig. 3. Instances of synthetic images used for the evaluation of robustness to blur and noise. On each image, the circular ROIs and the corresponding detected directionalities are shown. The top row shows images consisting of bars with thickness of 8 pixels (a), 12 pixels (b), and 16 pixels (c). The middle row shows images consisting of 12-pixel thick bars after applying Gaussian noise with standard deviation equal to 6000 (d), 12000 (e) and 1800 (f). The bottom row shows consisting of 12-pixel thick bars after applying blur with average kernels of pixel size 7×7 (g), 13×13 (h) and 19×19 (i).

B. Robustness of directionality estimation to Gaussian noise

The results of the tests of our texture directionality estimation algorithm with respect to its robustness to Gaussian noise are presented here. In Fig. 4, the average and maximum DDE is plotted against the noise standard deviation. Generally speaking, the directionality estimation algorithm seems sensitive to noise. In fact, there is no error only for noise standard deviation below 4000, which is below the lowest binning level (please observe that, since $0 - 65535$ is the intensity value range, which is grouped into 16 bins, each bin represents consecutive 4096 intensity values). Above 4000, the estimation error seems to grow proportionally to noise for both the average and maximum DDE plot. Larger errors for thicker bars are due to a lower incidence of the edges in the ROI, since they mainly carry the directionality information. Despite the decrease of the directionality estimation accuracy with the increasing of Gaussian noise, it is important to observe that the average DDE values remain limited to $1.23°$ for considered range of noise standard deviations. This is an acceptable error level, considering that 1-degree sampling was used for the directionality in the GLCM computation.

C. Robustness of directionality estimation to image blur

The results of the tests of our texture directionality estimation algorithm with respect to its robustness to blur are presented here. In Fig. 5, the average and maximum DDE is plotted against the average filter kernel size. The directionality estimation algorithm does not seem to be significantly affected by image blur. The average DDE for the bars of thickness

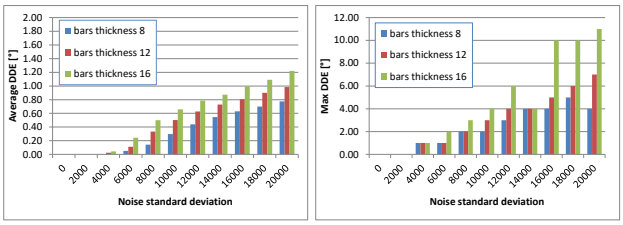

Fig. 4. Average (left) and maximum (right) Directionality Detection Error in function of the standard deviation of zero-mean Gaussian noise.

12 and 16 does not exceed $0.01°$ degrees, and the maximum DDE does not exceed $3°$. For bars of thickness 8, the average DDE does not exceed $0.01°$ degrees with averaging kernel sizes up to 11×11 pixels. On the other hand, with kernel sizes of 13×13 and up, the average DDE starts to grow without exceeding $0.14°$. The maximum DDE for bars of thickness 8 is limited to $4°$ with averaging kernel sizes up to 19×19, and it jumps to $26°$ with averaging kernel size of 21×21 pixels (the largest tested averaging kernel size). The only significant error increase was observed for bars of thickness 8, and it is due to the fact that such bar thickness is smaller than the size of averaging kernel. It should be noted that the observed low sensitivity to image blur is a very important property of the proposed texture directionality estimation algorithm, since image blur is one of the commonly used methods for noise reduction in images. In the future, the robustness to the other types of distortions as intensity nonuniformity [23] will be tested.

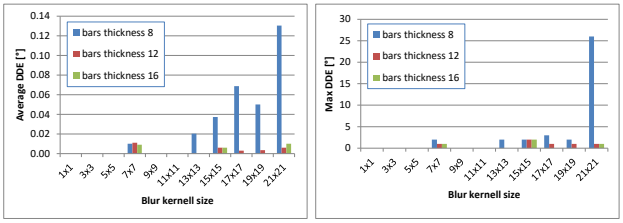

Fig. 5. Average (left) and maximum (right) Directionality Detection Error in function of the averaging kernel size.

D. Comparison with Fourier Transformation-based directionality estimation

The performance of our GLCM-based texture directionality estimation algorithm was compared to the well-established and widely used Fourier Transformation (FT)-based directionality estimation technique implemented in Fiji [7]. The comparison was based on the robustness of the directionality estimation with respect to image blur and Gaussian noise. The two algorithms were compared using the same synthetic images described earlier. The only difference is that, since the FT-based directionality estimation technique works only with rectangular ROIs, squared ROIs with edge size of 61 pixels were used rather than circular ROIs. In order to obtain the same total number of ROIs, the centers of the squared ROIs used for testing the FT-based texture directionality estimation

algorithm were defined so that they correspond to the centers of the circular ROIs used for testing the GLCM-based texture directionality estimation algorithm. In Fig. 6, the average

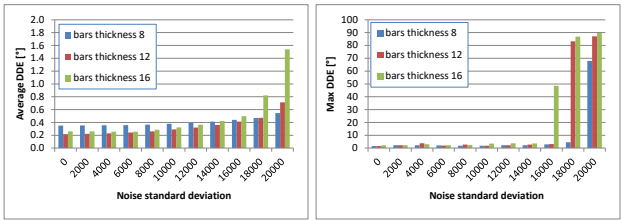

Fig. 6. Average (left) and maximum (right) Directionality Detection Error in function of the standard deviation of zero-mean Gaussian noise for the Fourier based method. .

and maximum DDE are plotted against the noise standard deviation for the FT-based directionality estimation algorithm. Based on the plots, the FT-based directionality estimation algorithm seems to be sensitive to Gaussian noise as well. The average DDE is not equal to zero even in absence of noise, and it increases not linearly with the increasing of the noise standard deviation. The average DDE does not exceed $0.5°$ for noise standard deviation values below 16000, while for higher noise standard deviation values it grows more rapidly. The maximum DDE behaves similarly, as it does not exceed $3.6°$ for noise standard deviation values below 16000, and then it rapidly grows. In comparison to the GLCM-based directionality estimation algorithm, the FT-based one is slightly less sensitive to Gaussian noise for noise standard deviation values below 16000. In Fig. 7, the average

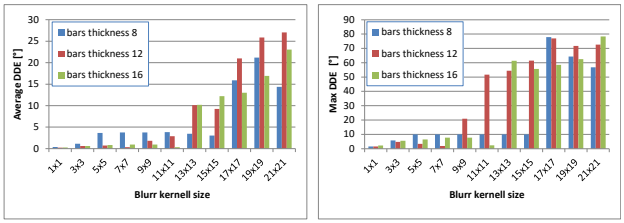

Fig. 7. Average (left) and maximum (right) Directionality Detection Error in function of the averaging kernel size for the Fourier based method. .

and maximum DDE are plotted against the averaging filter kernel size (i.e., blur level) for the FT-based directionality estimation algorithm. The obtained data shows that the FT-based directionality estimation algorithm is sensitive to blur as well. The average DDE is not equal to zero even in absence of blur, but this time its increasing with the size of the averaging kernel size is not fully monotonic. For averaging kernel sizes below 13×13 pixels, the average DDE does not exceed $3.8°$, while for larger averaging kernel sizes it grows rapidly. A similar behavior was found for the maximum DDE, which for averaging kernel sizes up to 7×7 pixels does not exceed $10°$. Even in this case, larger averaging kernel sizes results in a more rapid growth of the maximum DDE, not necessarily monotonic. Clearly, in comparison to the GLCM-based directionality estimation algorithm the FT-based one is far more sensitive to blur.

E. Example of applications

The texture directionality estimation algorithm was applied to microscopy images of actin fibers in fibroblast cells. In order to detect the locally varying directionality of texture in these images, each image has to be partitioned. The texture directionality images in Fig. 8 was estimated using circular overlapping tiles ($41 - pixel$ diameter). The local direction was superimposed on images as black lines. The resulting direcionality histograms are shown in polar coordinates. In

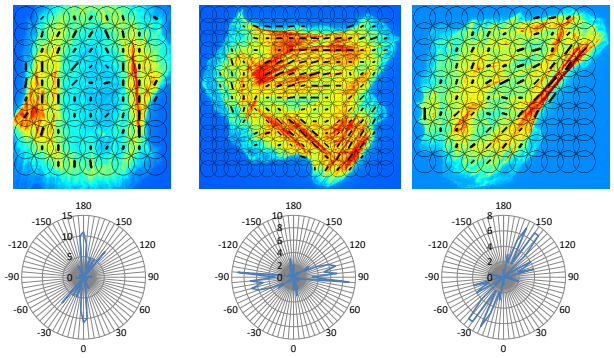

Fig. 8. Texture directionality estimation for three images of actin fibers in fibroblast cells. The tiled images are shown in pseudo colors, each tile containing the estimated directionality line with length proportional to DDC (top row); the corresponding polar histogram representing the directionality distribution is also shown for each image (bottom row).

the leftmost cell image from Fig. 8, two vertically oriented actin bundles are clearly noticeable. In fact, the largest bin of the corresponding polar histogram is very close to the vertical direction, and about 33% of the estimated texture directionalities are within $5°$ from the vertical direction. The center cell image from Fig. 8 contains several actin bundles with different directions. In fact, the corresponding polar histogram contains three dominating direction groups and not only one as before. The three direction groups are roughly centered at $45°$, $90°$ and $135°$, and about 50% of the estimated texture directionalities are within $10°$ from these three directions. Finally, one main actin bundle is clearly noticeable in the rightmost cell image from Fig. 8, along with several smaller actin fibers distributed across the cell. The largest bin in the corresponding polar histogram represents the estimated orientation of the main actin bundle ($\approx 140°$), whereas a few smaller bins also appear. The standard deviation of the estimated actin directionality is quite large in this case ($\approx 40°$). In general, the standard deviations of directionality estimates can be related to the directional distribution of actin during various cell states and hence to a quantitative imaging method for cell biology.

In conclusion, the above examples show that our texture directionality estimation algorithm enables quantitative characterization of texture directionality. Quantitative directionality estimation for cell images can find application in several biological studies, such as the ones focusing on the characterization of the arrangement of the proteins in the cytoskeleton of cells [10] and [11].

V. Conclusions

An interpolation-based GLCM computation technique was introduced in this paper. The technique allows GLCM computation for virtually any real-valued angle-offset pair, as opposed to current lattice-constrained GLCM computations. Based on the interpolation-based GLCM computation, a texture directionality estimation algorithm was introduced by finding the maximum of GLCM-derived correlation values over all angles and offsets.

The proposed GLCM-based directionality estimation algorithm was tested on synthetic images with known texture directionality, using progressive blur and additive Gaussian noise with increasing values of standard deviation. Results show robustness to both image blur and Gaussian noise. Our algorithm was also compared with the well-established FT-based directionality estimation algorithm, showing comparable performance with respect to noise, and much better performance with respect to blur. It is important to observe that our GLCM-based algorithm can be used with arbitrarily shaped regions of interest, unlike the FT-based one.

Our algorithm was also demonstrated on microscopy images of fibroblast cells. Results show a good match with the perceived texture directionality, and a quantitative characterization of texture directionality distribution with immediate interpretation is provided using polar histograms.

VI. Disclaimer

Commercial products are identified in this document in order to specify the experimental procedure adequately. Such identification is not intended to imply recommendation or endorsement by the National Institute of Standards and Technology, nor is it intended to imply that the products identified are necessarily the best available for the purpose.

Acknowledgment

We would like to thank Dr. Kiran Bhadriraju from the Nanoscale Metrology group in the Physical Measurements Laboratory at NIST and his colleagues from Material Measurements Laboratory at NIST for sharing the fibroblast cell images that were used in this paper.

References

[1] E. O. Olaniyi, A. A. Adekunle, T. Odekuoye, and A. Khashman, "Automatic system for grading banana using glcm texture feature extraction and neural network arbitrations," *Journal of Food Process Engineering*, vol. 40, no. 6, 2017.

[2] J. Neumann, U. Heilmeier, G. Joseph, F. Hofmann, W. Ashmeik, A. Gersing, N. Chanchek, B. Schwaiger, M. Nevitt, C. McCulloch *et al.*, "Texture analysis of t2 maps of the cartilage indicates differences in knee cartilage matrix in subjects with type 2 diabetes: data from the osteoarthritis initiative," *Osteoarthritis and Cartilage*, vol. 25, pp. S73–S74, 2017.

[3] K. Buch, B. Li, M. Qureshi, H. Kuno, S. Anderson, and O. Sakai, "Quantitative assessment of variation in ct parameters on texture features: pilot study using a nonanatomic phantom," *American Journal of Neuroradiology*, vol. 38, no. 5, pp. 981–985, 2017.

[4] R. M. Haralick, K. Shanmugam, and I. Dinstein, "Textural Features for Image Classification," *IEEE Transactions on Systems, Man, and Cybernetics*, vol. 3, no. 6, pp. 610–621, nov 1973. [Online]. Available: http://ieeexplore.ieee.org/document/4309314/

[5] P. M. Szczypiński, A. Klepaczko, and M. Kociołek, "Qmazda - software tools for image analysis and pattern recognition," in *Signal Processing: Algorithms, Architectures, Arrangements, and Applications (SPA), 2017*. IEEE, 2017, pp. 217–221.

[6] I. The MathWorks, "Create gray-level co-occurrence matrix from image - MATLAB graycomatrix." [Online]. Available: https://www.mathworks.com/help/images/ref/graycomatrix.html

[7] J. E. Cabrera, "Texture Analyzer, plugin for ImageJ/Fiji," 2006. [Online]. Available: https://imagej.nih.gov/ij/plugins/texture.html

[8] P. Bajcsy, J. Chalfoun, and M. Simon, "Functionality of web image processing pipeline," in *Web Microanalysis of Big Image Data*. Springer, 2018, pp. 17–40.

[9] T. scikit-image development, "Calculate the grey-level co-occurrence matrix." [Online]. Available: http://scikit-image.org/docs/dev/api/skimage.feature.html#skimage.feature.greycomatrix

[10] P. Hotulainen and P. Lappalainen, "Stress fibers are generated by two distinct actin assembly mechanisms in motile cells," *The Journal of Cell Biology*, vol. 173, no. 3, 2006.

[11] M. Théry, A. Pépin, E. Dressaire, Y. Chen, and M. Bornens, "Cell distribution of stress fibres in response to the geometry of the adhesive environment," *Cell Motility and the Cytoskeleton*, vol. 63, no. 6, pp. 341–355, jun 2006. [Online]. Available: http://www.ncbi.nlm.nih.gov/pubmed/16550544 http://doi.wiley.com/10.1002/cm.20126

[12] J.-Y. Tinevez, "Directionality (Fiji)," 2010. [Online]. Available: https://imagej.net/Directionality

[13] K. Jafari-Khouzani and H. Soltanian-Zadeh, "Radon transform orientation estimation for rotation invariant texture analysis." *IEEE transactions on pattern analysis and machine intelligence*, vol. 27, no. 6, pp. 1004–8, jun 2005. [Online]. Available: http://www.ncbi.nlm.nih.gov/pubmed/15945146

[14] P. Peng Jia, J. Junyu Dong, L. Lin Qi, and F. Autrusseau, "Directionality measurement and illumination estimation of 3D surface textures by using mojette transform," in *2008 19th International Conference on Pattern Recognition*. IEEE, dec 2008, pp. 1–4. [Online]. Available: http://ieeexplore.ieee.org/document/4761389/

[15] D. Feng, L. Chunlin, X. Cheng, and S. Wei, "Research of spectrum measurement of texture image," in *World Automation Congress 2012.*, 2012, pp. 163–165.

[16] R. Mester, "Orientation estimation: Conventional techniques and a new non-differential approach - IEEE Xplore Document," in *Signal Processing Conference, 2000 10th European*, 2000, pp. 3–6. [Online]. Available: http://ieeexplore.ieee.org.00000azm0aaa.han.p.lodz.pl/document/7075718/

[17] B. Julesz, "Experiments in the visual perception of texture." *Scientific American*, vol. 232, no. 4, pp. 34–43, apr 1975. [Online]. Available: http://www.ncbi.nlm.nih.gov/pubmed/1114309

[18] W. Lu, "Adaptive noise attenuation of seismic image using singular value decomposition and texture direction detection," in *Proceedings. International Conference on Image Processing*, vol. 2. IEEE, 2002, pp. 465–468. [Online]. Available: http://ieeexplore.ieee.org/document/1039988/

[19] W. Hu, H. Li, C. Wang, S. Gou, and L. Fu, "Characterization of collagen fibers by means of texture analysis of second harmonic generation images using orientation-dependent gray level co-occurrence matrix method," *Journal of Biomedical Optics*, vol. 17, no. 2, p. 026007, feb 2012. [Online]. Available: http://www.ncbi.nlm.nih.gov/pubmed/22463039

[20] K. R. Castleman, *Digital image processing*. New Jercey: Prentice Hall, 1996.

[21] The MathWorks Inc., "Properties of gray-level co-occurrence matrix - MATLAB graycoprops." [Online]. Available: http://www.mathworks.com/help/images/ref/graycoprops.html

[22] M. Kociolek and A. Cardone, "Haralick Based Directionality Map - source code repository," 2016. [Online]. Available: https://github.com/marcinkociolek/HaralickBasedDirectionalityMap

[23] A. Materka and M. Strzelecki, "On the importance of mri nonuniformity correction for texture analysis," in *2013 Signal Processing: Algorithms, Architectures, Arrangements, and Applications (SPA)*, Sept 2013, pp. 118–123.